https://doi.org/10.18524/1810-4215.2025.38.343164

SPECTROSCOPIC STUDY OF THE POST-AGB BINARY HR 4049

Sh. T. Nurmakhametova[1], N. L. Vaidman[1,2], A. S. Miroshnichenko[1,2,3], A. T. Agishev[1], A. A. Khokhlov[1]

[1] Al-Farabi Kazakh National University, Al-Farabi Ave, 71, 050040, Almaty, Kazakhstan, *shahidanurmahametova@gmail.com; aldiyar.agishev@gmail.com; kh.azamat92@gmail.com*

[2] Fesenkov Astrophysical Institute, Observatory 23, 050020, Almaty, Kazakhstan, *nva1dmann@gmail.com*

[3] Department of Physics and Astronomy, University of North Carolina at Greensboro, Greensboro, USA, *a_mirosh@uncg.edu*

ABSTRACT. We present a new spectroscopic study of HR 4049, a post-AGB star in a binary system, based on échelle spectra obtained between 2019/03/19 and 2025/04/08 with the 0.81 m telescope of the Three College Observatory (North Carolina, USA) at a resolution of $R \approx 12{,}000$. A cross-correlation analysis of 83 spectra in the 4760–4780 Å range yielded the following orbital parameters: period $P = 428.47 \pm 0.01$ days, eccentricity $e = 0.29 \pm 0.01$, argument of periastron $\omega = 242.3° \pm 0.3°$, epoch of periastron $T_0 = 2{,}458{,}383.2 \pm 0.6$, systemic radial velocity $\gamma = -30.12 \pm 0.09$ km s^{-1}, and semi-amplitude $K_1 = 15.52 \pm 0.13$ km s^{-1}. Using the Gaia DR3 parallax ($d = 1397^{+176}_{-168}$ pc) and the average maximum brightness ($m_v = 5.35$ mag), the luminosity was estimated as $\log(L/L_\odot) = 4.22 \pm 0.12$, consistent with an initial mass of 3-4 $M_\odot$. The mass function combined with likely orbital inclinations implies current masses of ~ 0.75 $M_\odot$ for the primary and 0.70–0.82 $M_\odot$ for the secondary. These results confirm the long-term orbital stability of HR 4049 and provide new constraints on the properties of post-AGB binaries.

Keywords: spectroscopy; binary stars; emission-line stars; post-AGB stars; circumstellar matter.

АНОТАЦІЯ. Ми представляємо нове спектроскопічне дослідження HR 4049, зорі після AGB у подвійній системі, на основі échelle-спектрів, отриманих у 2019/03/19 – 2025/04/08 рр. за допомогою телескопа діаметром 0.81 м Обсерваторії Трьох Коледжів (Північна Кароліна, США) з роздільною здатністю $R \approx 12\ 000$. Кроскореляційний аналіз 83 спектрів у діапазоні 4760–4780 Å дозволив визначити орбітальні параметри: період $P = 428{,}47 \pm 0{,}01$ доби, ексцентриситет $e = 0{,}29 \pm 0{,}01$, аргумент періастра $\omega = 242.3° \pm 0.3°$, епоха періастра $T_0 = 2{,}458{,}383.2 \pm 0.6$, системна швидкість $\gamma = -30.12 \pm 0.09$ км с$^{-1}$ та напівамплітуда $K_1 = 15.52 \pm 0.13$ км с$^{-1}$. Використовуючи паралакс Gaia DR3 ($d = 1397^{+176}_{-168}$) та середню максимальну зоряну величину ($m_v = 5{,}35$ mag), світність оцінено як $\log(L/L_\odot) = 4{,}22 \pm 0{,}12$, що відповідає початковій масі 3–4 $M_\odot$. Масова функція у поєднанні з вірогідними нахилами орбіти вказує на сучасні маси ~ 0.75 $M_\odot$ для первинної компоненти та 0,70–0,82 $M_\odot$ для вторинної. Отримані результати підтверджують довготривалу орбітальну стабільність HR 4049 та встановлюють нові обмеження на властивості пост-AGB подвійних систем.

Ключові слова: спектроскопія; подвійні зорі; зорі з емісійними лініями; зорі після AGB ; навколозоряна речовина.

1. Introduction

Post-AGB stars are an intermediate evolutionary stage of low– and intermediate–mass stars ($\sim$ 0.8–8 $M_\odot$) after the Asymptotic Giant Branch (AGB) phase and before becoming Planetary Nebulae (PN). At this stage, the star has lost most of its outer envelope due to strong stellar winds, leaving behind a hot core surrounded by an expanding circumstellar shell of gas and dust.

This phase is very short in astrophysical terms (10^3–10^5 years) which makes post-AGB stars rare. Their luminosities are typically around 10^3–10^4 $L_\odot$, with effective temperatures ($T_{\rm eff}$) ranging from about 3000 K to over 100,000 K as they evolve towards higher temperatures (Miller Bertolami 2016).

One of the most remarkable post-AGB objects is HR 4049 (HD 89353, AG Ant), a spectroscopic binary in Antlia. Its high $T_{\rm eff} \approx 7500$ K (Bakker et al. 1998), complicates abundance work because metal lines are weak. HR 4049 shows an extreme iron underabundance, [Fe/H]$= -4.8$ dex (Van Winckel et al. 1995), together with a strong infrared excess and a UV deficit attributable to dust from past mass loss (Andrews, Lépine 2013). Selective depletion is common among post-AGB binaries with circumbinary disks; HR 4049 is among the most extreme cases. As a result, its optical spectrum contains very few measurable metal lines.

Spectroscopic monitoring revealed radial velocity (RV) variations with a 429–430 day period (Bakker et al. 1998), confirming its binarity with a faint companion (Andrews, Lépine 2013). The companion is likely an M–type main-sequence star with $T_{\rm eff} \approx 3500$ K, $R \approx 0.6 R_{\odot}$ and the compact orbit has $a \sin i \approx 0.6$ AU (Bakker et al. 1998).

The system also hosts a stable circumbinary disk with a bright ring (Andrych et al. 2023). The double-peaked Hα profile follows the orbital phase, suggesting accretion activity (Gorlova et al. 2012), while star–disk interactions may cause severe photospheric depletion of volatile elements (Oomen et al. 2019).

The aim of this study was to refine the orbital parameters of HR 4049 using new RV data and test for possible long-term changes. We recalculated P, γ, ω, e, K, and T_0, thereby improving constraints on the orbital architecture and fundamental properties of this post-AGB binary.

2. Observations, Data Reduction and Analysis

We obtained 83 spectra of HR 4049 between 2019/03/19 and 2025/04/08 with the 0.81 m telescope at the Three College Observatory (North Carolina, USA), equipped with an échelle spectrograph manufactured by Shelyak Instruments [1] and an ATIK-460EX detector. The setup provides $R \sim 12{,}000$ over 3800-7900 Å, with S/N ratios in the continuum up to ∼300 for typical combined exposure times of ∼1 hour in the 4500-5500 Å range. Wavelength calibration using 800-1000 ThAr lines yields an RV precision of ∼300 m s^{-1}. Spectra were reduced with standard IRAF échelle routines (bias subtraction, flat-fielding, optimal extraction, and continuum normalization).

To achieve the main objectives of this study, we applied several complementary methods. To measure RV values, we applied the cross-correlation method implemented in the IRAF/RVSAO 2.0 package, using one high-S/N spectrum as a template and focusing on the C I multiplet in the 4760–4780 Å region.

[1] `https://shelyak.com`

Periodogram analysis of the RV data was then performed with the Lomb–Scargle (LS) algorithm (Scargle 1982), which is well suited for unevenly sampled observations and allowed us to identify the dominant periodicity of the system.

Subsequently, we modeled the RV curve with our Python pipeline (NumPy, Pandas, Matplotlib, SciPy) and performed Bayesian inference using the affine-invariant ensemble sampler `emcee` (Foreman-Mackey et al. 2013). The RV+MCMC code is documented in Vaidman et al. (2025) and has already been applied in Nurmakhametova et al. (2025) and in Vaidman et al. (2025); we follow the same workflow here to obtain the most probable orbital elements—period, systemic velocity, semi-amplitude, eccentricity, and argument of periastron—with robust uncertainties.

3. Results

In the 4760–4780 Å region, the spectra of HR 4049 clearly show the neutral–carbon multiplet (top panel of Fig. 1). HR 4049 is strongly depleted in refractory elements, so its optical spectrum contains comparatively few clean metal lines; many wavelength ranges are either line–poor or affected by blends and circumstellar features. The chosen window, however, contains several relatively strong, well–isolated C I lines with stable, symmetric profiles and minimal telluric contamination. The phase–resolved cross–correlation map (bottom panel of Fig. 1) demonstrates coherent Doppler shifts of these lines with orbital phase, confirming that this set is well suited to precise RV measurements and a subsequent orbital analysis.

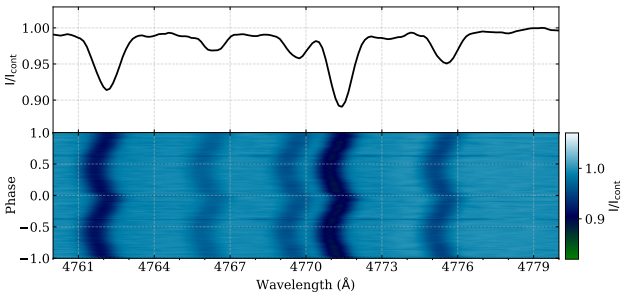

Figure 1: Top panel: Spectrum of HR 4049 in the 4760–4780Å region. Bottom panel: Phase-resolved cross-correlation map.

Table 1 compares the orbital parameters of HR 4049 obtained in this work with previous studies. Our analysis confirms the overall consistency of the system's orbital characteristics with earlier results, while providing an improved precision. Small differences in systemic velocity are most likely related to the choice of template spectrum and reference frame. The refined

parameters strengthen the evidence for the long-term stability of the binary system.

Table 1: Comparison of orbital parameters.

	Bakker et al. (1998)	**Oomen et al. (2019)**	**This work**
P	430.7 ± 0.3	430.6 ± 0.1	428.47 ± 0.01
T_0	$46\,746.6 \pm 2.4$	$47\,176.6 \pm 3.8$	$58\,383.2 \pm 0.6$
e	0.30 ± 0.01	0.30 ± 0.01	0.29 ± 0.01
ω	237.2 ± 2.3	236.5 ± 3.5	242.3 ± 0.3
γ	-32.1 ± 0.1	-31.9 ± 0.2	-30.1 ± 0.1*
K_1	15.96 ± 0.19	16.6 ± 0.2	15.52 ± 0.13
$f(m)$	0.16 ± 0.01	0.18 ± 0.01	0.15 ± 0.01
N	60	86	83

Notes. (1) Orbital period (days); (2) periastron epoch for the elliptical orbit and time of superior conjunction (at γ RV) for the circular orbit (HJD -2,400,000); (3) eccentricity; (4) argument of periastron (degrees); (5) systemic RV (km s^{-1}); (6) semi-amplitude of the RV variations of the visible component ($km\,s^{-1}$); (7) mass function ($M_\odot$); (8) number of spectra used in the orbit calculation.

* The value is obtained from the RV template, with the systemic velocity determined relative to the template spectrum and reported in the heliocentric frame.

To determine the orbital period from our irregularly sampled velocities, we computed LS periodogram as a first-order approach. For improved accuracy, we also included archival spectra from Bakker et al. (1998), which complement our recent observations and help to extend the temporal baseline of RV measurements. As shown in Fig. 2, the resulting LS spectrum displays a dominant peak at $P = 428.47$ d. We therefore adopt this period as the starting point for the orbital analysis. With P fixed at this value, we then fit a Keplerian model with free parameters K, e, ω, T_0, and the systemic velocity γ, ensuring a consistent solution across all available datasets.

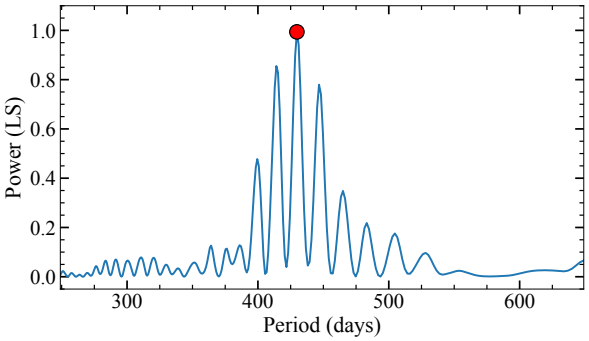

Figure 2: Lomb–Scargle periodogram. The red dot marks the global maximum at $P = 428.47 \pm 0.01$ d.

Fig. 3 compares this model to the RV time series. The fit reproduces both the amplitudes and the evident asymmetry of the RV curve, indicating a non-zero eccentricity. In this workflow, the LS periodogram serves to identify the fundamental timescale under uneven sampling, while the subsequent Keplerian fit accounts for the non-sinusoidal shape of eccentric orbits and yields physically interpretable parameters.

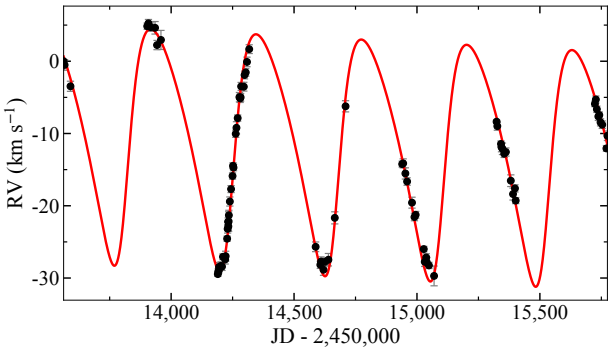

Figure 3: Radial velocities as a function of time, plotted as JD$-2{,}450{,}000$ (black points with 1σ error bars), together with the best-fitting Keplerian model (red curve).

To illustrate the coherence of the solution, Fig. 4 shows the phase-folded velocities at the same period together with the best-fitting Keplerian model. The residuals, normalized by their formal uncertainties, scatter symmetrically about zero with no visible structure, supporting the adequacy of the single-orbit description and the robustness of the adopted period.

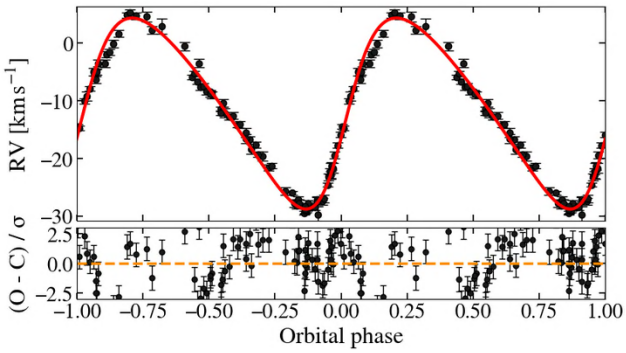

Figure 4: Radial velocity variations of HR 4049 as a function of orbital phase. Top panel: Black points show the observed heliocentric RVs; the red curve represents the best-fitting Keplerian model. Bottom panel: Normalised residuals $(O-C)/\sigma$; the orange dashed line marks zero. The plot shows all $N = 83$ measurements; the eccentric Keplerian fit yields a reduced $\chi^2_\nu = 1.69$.

We estimated the luminosity of HR 4049 at its maximum optical brightness using the observed visual magnitude $m_V = 5.35$ mag (Waelkens et al. 1991; Rufener

& Bartholdi 1982; Lake 1965). For the distance, we adopted the *Gaia* DR3 value $d = 1397^{+176}_{-168}$ pc as determined by Bailer-Jones et al. (2021, Vizier catalogue I/352), providing a reliable geometric basis for our estimates. To convert the apparent magnitude to bolometric luminosity, we applied a bolometric correction of $BC_V = 0.02$, appropriate for an effective temperature of $T_{\rm eff} = 7500$ K according to the calibration of Pecaut & Mamajek (2013).

Assuming a modest interstellar reddening of $E(B-V) < 0.07$, we obtained $\log(L/L_\odot) = 4.13$, whereas adopting a slightly higher color excess of $E(B-V) = 0.20$ yields $\log(L/L_\odot) = 4.30$ (Green et al. 2019). These values define the plausible luminosity range, and for the subsequent discussion we adopt the mean estimate $\log(L/L_\odot) = 4.22 \pm 0.12$, which agrees, within the quoted uncertainties, with previous determinations reported by Oudmaijer et al. (2022).

When placed on the Hertzsprung–Russell (HR) diagram (Fig. 5), HR 4049 occupies a position along the post–AGB evolutionary tracks corresponding to progenitors of approximately 3–4 $M_\odot$. This location is consistent with the phase of nearly constant luminosity and gradually increasing effective temperature that characterizes the final stages of post–AGB evolution, supporting the classification of HR 4049 as a well–advanced post–AGB object.

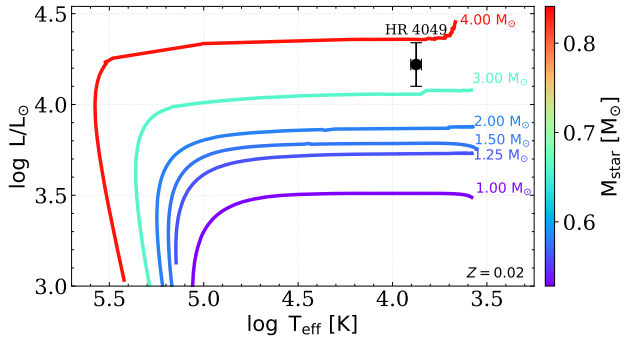

Figure 5: HR diagram of post-AGB tracks for initial masses 1–4 $M_\odot$ at $Z = 0.02$ (Miller Bertolami 2016). The color bar shows the present stellar (core) mass. The black symbol marks HR 4049.

The mass function derived from our orbital solution (Table 1) provides a valuable quantitative constraint on the possible masses of both stellar components and thus serves as an important diagnostic of the system's nature. For representative orbital inclinations in the range $i = 60°$–$75°$ (Dominik et al. 2003; Oomen et al. 2018), the resulting mass of the primary component is estimated as $M_1 \approx 0.75\,M_\odot$, a value that agrees very well with theoretical expectations for evolved post–AGB remnants. In particular, according to the post–AGB evolutionary calculations of Blöcker (1995), stars with initial main–sequence masses between $3-5\,M_\odot$ are expected to leave the AGB phase with core masses in the range $0.605-0.889\,M_\odot$. The mass we infer for the primary thus falls comfortably within this theoretical interval, further strengthening the internal consistency and physical plausibility of our orbital solution. The inferred $M_2 \approx 0.70$–$0.82\,M_\odot$ is difficult to reconcile with a late-M dwarf; this range is more consistent with either an early-K main-sequence star or a compact white dwarf. The corresponding mass of the unseen secondary component therefore remains compatible with both possibilities. It should be emphasized that this range is still strongly dependent on the adopted inclination, and the steep sensitivity of M_2 to i clearly illustrates how delicate and model–dependent mass determinations can be for single–lined spectroscopic binaries with unresolved companions (Fig. 6).

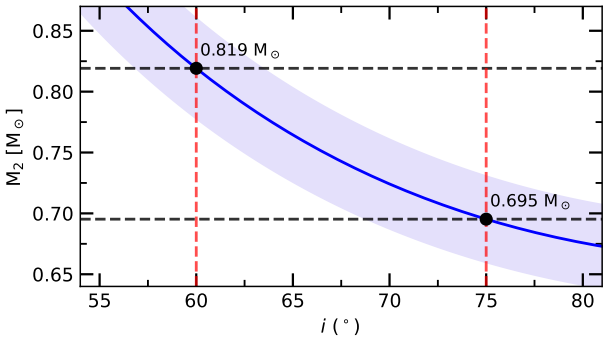

Figure 6: Mass of the secondary component M_2 as a function of the orbital inclination i. The solid blue line shows the best-fit solution for the mass function $f(M) = 0.15$, with the shaded region representing the uncertainty (± 0.01). The dashed horizontal line marks the assumed primary mass $M_1 = 0.75 \pm 0.05\,M_\odot$. Red dashed vertical lines highlight the solutions at $i = 60°$ and $i = 75°$.

4. Conclusions

We carried out a spectroscopic analysis of the post-AGB binary HR 4049 using 83 échelle spectra obtained between 2019 and 2025. The RV measurements of the C I multiplet lines allowed us to refine the orbital parameters, which are consistent with previous determinations but now have improved precision. Placing HR 4049 on the HR diagram confirms that it follows post-AGB evolutionary tracks for progenitors of 3-4 M⊙, while the derived mass function constrains the present-day component masses to ∼0.75 M⊙ for the primary and 0.70–0.82 $M_\odot$ for the secondary. These results confirm the system's long-term orbital stability and provide important constraints for understanding post-AGB binaries with circumbinary disks.

Despite this progress, several open problems remain.

The origin of the extreme iron deficiency in HR 4049 is still unclear and likely linked to complex depletion and re-accretion processes in the circumbinary environment. Moreover, as HR 4049 is in a rare and short-lived evolutionary phase, a follow-up spectroscopic and photometric monitoring will be essential to trace its variability, chemical composition, and dynamical evolution. Future monitoring of HR 4049 will be crucial for tracing possible secular variations in orbital and spectral properties.

Funding. This research has was funded by the Science Committee of the Ministry of Science and Higher Education of the Republic of Kazakhstan (Grant No. AP19175392).

Acknowledgements. This research has made use of the SIMBAD database, operated at CDS, Strasbourg, France; SAO/NASA ADS, ASAS, and Gaia data products. This paper is partly based on observations obtained at the 0.81 m of the Three College Observatory (North Carolina, USA). A.M. acknowledges technical support from Dan Gray (Sidereal Technology Company), Joshua Haislip (University of North Carolina Chapel Hill), and Mike Shelton (University of North Carolina Greensboro), as well as funding from the UNCG College of Arts and Sciences and Department of Physics and Astronomy.

References

Andrews J., Lépine S.: 2013, *Astron. Astrophys.,* **551**, A76.

Andrych K., Kamath D., Kluska J., Van Winckel H., Ertel S., Corporaal A.: 2023, *Mon. Not. R. Astron. Soc.,* **524**, 4168.

Bakker E.J., Lambert D.L., Van Winckel H., McCarthy J.K., Waelkens C., Gonzalez G.: 1998, *Astron.Astrophys.,* **336**, 263.

Bailer-Jones C.A.L., Rybizki J., Fouesneau M., Demleitner M., Andrae R.: 2021, *Astron. J.,* **161**, 147.

Blöcker T.: 1995, *Astron. Astrophys.,* **299**, 755.

Dominik C., Dullemond C.P., Cami J., van Winckel H.: 2003, *Astron. Astrophys.,* **397**, 595–609.

Foreman-Mackey D., Hogg D.W., Lang D., Goodman J.: 2013, *Publ. Astron. Soc. Pac.,* **125**, 306.

Gorlova N., Van Winckel H., Gielen C., Raskin G., Prins S., Pessemier W., Waelkens C., Frémat Y., Hensberge H., Dumortier L., et al.: 2012, *Astron. Astrophys.,* **542**, A27.

Green G.M., Schlafly E.F., Zucker C., Speagle J.S., Finkbeiner D.P.: 2019, *Astrophys. J.,* **887**, 93.

Lake R.: 1965, *Mon. Not. Astron. Soc. S. Afr.,* **24**, 41.

Miller Bertolami M.M.: 2016, *Astron. Astrophys.,* **588**, A25.

Nurmakhametova S.T., Vaidman N.L., Miroshnichenko A.S., Khokhlov A.A., Agishev A.T., Yermekbayev B.S., Danford S., Aarnio A.N.: 2025, *Galaxies,* **13**(2), 26.

Oomen G.-M., Van Winckel H., Pols O., Nelemans G.: 2019, *Astron. Astrophys.,* **629**, A49.

Oomen G.-M., Van Winckel H., Pols O., Nelemans G., Escorza A., Manick R., Kamath D., Waelkens C.: 2018, *Astron. Astrophys.,* **620**, A85.

Oudmaijer R.D., Jones E.R.M., Vioque M.: 2022, *Mon. Not. R. Astron. Soc.: Lett.,* **516**, L61.

Pecaut M.J., Mamajek E.E.: 2013, *Astrophys. J. Suppl. Ser.,* **208**, 9.

Rufener F., Bartholdi P.: 1982, *Astron. Astrophys. Suppl. Ser.,* **48**, 503.

Scargle J.D.: 1982, *Astrophys. J.,* **263**, 835.

Van Winckel H., Waelkens C., Waters L.B.F.M.: 1995, *Astron. Astrophys. Lett.,* **293**, L25.

Vaidman N.L., Nurmakhametova S.T., Miroshnichenko A.S., Khokhlov S.A., Agishev A.T., Khokhlov A.A., Ashimov Y.K., Yermekbayev B.S.: 2025, *Galaxies,* **13**(5), 101.

Vaidman N.L., Miroshnichenko A.S., Zharikov S.V., Khokhlov S.A., Agishev A.T., Yermekbayev B.S.: 2025, *Galaxies,* **13**(3), 47.

Waelkens C., Lamers H.J.G.L.M., Waters L.B.F.M., Rufener F., Trams N.R., Le Bertre T., Ferlet R., Vidal-Madjar A.: 1991, *Astron. Astrophys.,* **242**, 433.